ELSEVIER

Journal of Wind Engineering
and Industrial Aerodynamics 84 (2000) 65–85

JOURNAL OF wind engineering AND industrial aerodynamics

www.elsevier.com/locate/jweia

Flow visualization of conical vortices on flat roofs with simultaneous surface pressure measurement

D. Banks[a,*], R.N. Meroney[a], P.P. Sarkar[b], Z. Zhao[b], F. Wu[b]

[a]*Fluid Mechanics and Wind Engineering Program, Civil Engineering Department, Colorado State University, Fort Collins, CO 80523, USA*

[b]*Wind Engineering Research Center, Department of Civil Engineering, Texas Tech University, Lubbock, TX 79409-1023, USA*

Received 2 September 1997; received in revised form 15 December 1998; accepted 9 June 1999

Abstract

Wind tunnel and full-scale pressure studies of flow over low-rise buildings have repeatedly shown that on the roof, the largest mean and peak suction values are observed for taps beneath the conical "delta-wing type" corner vortices that occur for oblique winds. To better understand the flow mechanism which produces these negative pressure coefficients, a flow visualization study of conical vortex behaviour was performed in the wind tunnels of Colorado State University (CSU) and at full scale at Texas Tech University (TTU). The mean position and size of the vortices as a function of wind direction is presented. Pressures were also simultaneously measured beneath the vortex visualization plane in the wind tunnel for the worst case wind directions. These pressure profiles were correlated with the digitally enhanced images of the vortex flow. The greatest suction was found to follow directly beneath the moving vortex core. For smooth flow, the magnitude of the suction beneath the core was seen to vary inversely with the vortex size, but no relationship between vortex size and suction could be seen for turbulent flow.

Keywords: Bluff body; Delta-wing vortices; Low rise; Square prism

1. Introduction

Many studies have shown that the worst mean and peak suctions on flat building roofs occur for cornering or oblique wind angles (see, for example, Ref. [1]). At such

* Corresponding author. Tel.: +1-970-491-8574; fax: +1-970-491-8671.
E-mail address: db@lamar.colostate.edu (D. Banks)

0167-6105/00/$ - see front matter
PII: S0167-6105(99)00044-6

Nomenclature

C_p	pressure coefficient $= (P - P_{ref})/\frac{1}{2}\rho U_{ref}^2$
$C_{\bar{p}}, C_{\sigma_p}, C_p^{\vee}$	mean, rms, and peak negative values of the pressure coefficient time series $C_p(t)$, where $C_p(t) = (P(t) - P_{ref})/\frac{1}{2}\rho U_{ref}^2$
h	height or distance of the vortex core above the roof surface
h_0	height of the vortex core above the roof surface at the roof apex ($x = 0$)
H	height of building or prism
P	static pressure
r	distance from the vortex core along the roof surface in the y-direction.
U_{ref}	mean flow velocity at a reference point away from the model
u, v, w	flow velocity fluctuations in the direction of (u) or normal to (v,w) mean flow vector
x	distance from the apex or leading edge corner, measured along the leading edge
y	Distance from the leading edge wall, along a line normal to the leading edge
$y_{1/2}$	half-width of the y-direction pressure profile suction peak
z	distance above the roof surface
z_m	theoretical vortex core height above the roof surface, used in potential flow theory
ρ	air density
ω	wind angle; 90° is normal to the leading edge
ϕ	angle formed along the roof surface with respect to the leading edge
ϕ_C	angle formed between the ray of the mean vortex core position and the leading edge
$\phi_{\bar{p}}, \phi_{\sigma_p}, \phi_p^{\vee}$	angles formed between the leading edge and the rays of highest-$C_{\bar{p}}$, C_{σ_p}, and $C_p^{\vee}$
$\Delta x, \Delta h, \Delta y$	incremental change in the quantities x, h, or y.

Most of these symbols are depicted in Figs. 3 or 6.

angles, conical or delta wing vortices form along the roof edges (see Fig. 1). Interest in the behaviour of these vortices has been heightened by the unexpected discrepancy between the peak and RMS surface pressures measured under these vortices for full-scale tests and those measured for model scale tests (see, for example, Ref. [2]), though recent refinements to the wind tunnel boundary layer simulation appear to have reduced or eliminated this discrepancy [3].

In 1994, Tieleman wrote that "no comprehensive results are available for the variations of surface pressures on top surfaces of prisms, immersed in turbulent boundary layers, with the nature of the incident flow (mean flow profile, turbulence

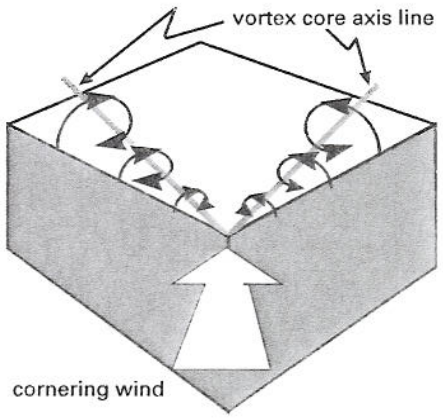

Fig. 1. Conical "delta-wing" corner vortices.

intensity and turbulence scales)", adding that discrepancies between extreme pressures measured in the separated flow zones of full scale and model scale building roofs were "attributed to the inadequate simulation of lateral velocity fluctuation". [4]. The paper went on to show that higher model scale peak suctions could be induced by altering the upstream spire-roughness arrangement to increase the lateral turbulence intensity.

Lateral turbulence intensity had also been cited by Letchford and Mehta [5] as playing an important role in pressure fluctuations for quartering winds. This conclusion was based upon the similarity between the shape of pressure eigenvectors under the vortices and the pattern of $dC_{\hat{p}}/d\omega$ values. The latter term, an indication of surface pressure dependence upon mean lateral wind direction, is linked to surface pressure fluctuations in quasi-steady theory by a term which couples this derivative with lateral turbulence intensity [6]. Note, however, that this latter study concluded that the quasi-steady theory fails fundamentally to deal with flow distortion due to building generated turbulence.

Since 1994, several studies have addressed the link between incident flow and surface pressures, and in particular the issue of the effects of lateral turbulence. Ref. [6] compared simultaneous upstream laser doppler anemometer (LDA) measurements of u-v-w velocity fluctuations and model surface pressures. These flow velocity measurements were taken quite close to the building, at distances upstream of 1/2 and 1/10th of the building height. Conditional sampling was used to isolate the effects of instantaneous wind direction on C_p values. The conclusion was that extremes in pressures were associated with large excursions in lateral velocity, specifically excursions toward a flow normal to the wall.

This agrees in essence with the full-scale work of Zhao [7] for normal flows, who also compared roof pressures with wind flow and direction immediately upstream of the roof, and concluded that the local, non-conventional C_p (where pressures are normalized by the local wind speed to isolate wind direction effects) assumes peak suction values during fast and large fluctuations in lateral wind direction.

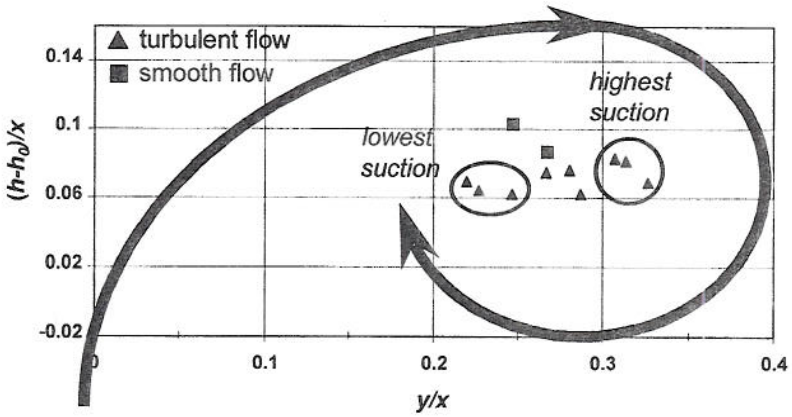

Fig. 2. Suction versus core position (adapted from Ref. [9]).

Kawai and Nishimura [8] have also simultaneously measured roof suctions and upstream velocities for a flat roof low rise model building. They concluded, based on the correlation of suction fluctuation over the entire roof, that the dual conical vortices sway in unison. They also saw a correlation between suction fluctuation in the re-attachment zone and approaching low-frequency lateral turbulence, leading them to conclude that the lateral component of approaching turbulence amplifies the sway of the vortex axes, causing increases in low-frequency suction fluctuations.

While these studies have made progress in linking flow characteristics to surface pressures, Marwood and Wood wrote in 1996 that "the mechanism linking vortex structure and surface pressure is little understood". [9] This comment prefaced a report on a study in which surface pressures and flow velocities at a point within the vortex core were simultaneously sampled. Conditional analysis of the velocities at various points in the separated flow associated with peak and minimum suctions revealed some of the average separated flow characteristics associated with the largest and smallest suctions. For example, Fig. 2 (adapted from Ref. [9]) shows that the higher suctions were generally associated with larger vortices for turbulent flow.

This study continues, in the same vein as Refs. [8,9], to pursue a link between vortex behaviour and surface pressures. It is hoped that once this link is better understood, the flow characteristics controlling vortex behaviour can be more directly associated with roof top surface pressure events, and the nature of the breakdown in the quasi-steady theory's link between flow parameters (such as lateral turbulence intensity) and surface pressures can be ascertained.

This work is being carried out at Colorado State University and Texas Tech University as part of a Co-operative Program in Wind engineering (CPWE). The investigation of wind flow around low-rise buildings is one of the three areas of emphasis of this 5-year research program (1995–1999).

This paper discusses the results of visualization studies that have been performed at both TTU and CSU to determine the position and size of the vortex as a function of incident wind characteristics, especially wind direction. In addition, surface pressures

were simultaneously measured during the wind-tunnel visualization, providing a clear link between instantaneous surface pressures and vortex behaviour.

2. Experimental procedures

2.1. Preliminary flow visualization

Initial wind tunnel tests were performed for smooth flow in the CSU Environmental Wind Tunnel (EWT), which is a non-recirculating tunnel with a 3.7 m × 2.1 m cross-section. Several different cuboidal models, ranging from 450 mm to 1.2 m on any given side, were mounted above the tunnel floor boundary layer. A laser light sheet was used to illuminate a plane within the vortex core region, and images were recorded on an SVHS camera. The laser is a Coherent Innova 70-5 argon ion water-cooled laser, and it was operated in multi-line mode for these tests. It has a nominal maximum output power of 5 W, but was generally run at or below 1 W for these tests. The laser beam was focused and spread into a sheet by lenses mounted on the tunnel ceiling. Glycerin smoke was introduced through holes near the leading corner (apex) of a model's roof.

The light sheet was positioned at various distances from the apex, usually normal to the leading edge. It was found that the mean core position follows a straight line, beginning at the apex and running along the leading edge. The position of this core-line, or ray, can be defined by a vortex core angle (ϕ_C) and a height ratio (h/x), as shown in Fig. 3. It should be noted that at $x = 0$, the core has an initial finite displacement above the apex of around $h_0 = 2$ mm (Fig. 4). Since the core rises very slowly ($\Delta h/\Delta x = 7$ mm/100 mm for $\omega = 45°$), this will distort h/x values by over 10% for $x < 300$ mm. This is important for comparing the normalized results of many vortex visualization studies, which are often carried out on small (100–200 mm long) models. This study normalizes the vortex core height using $(h - h_0)/x$. Fig. 3 also illustrates the definition of the wind angle (ω) used in this study. Winds normal to the

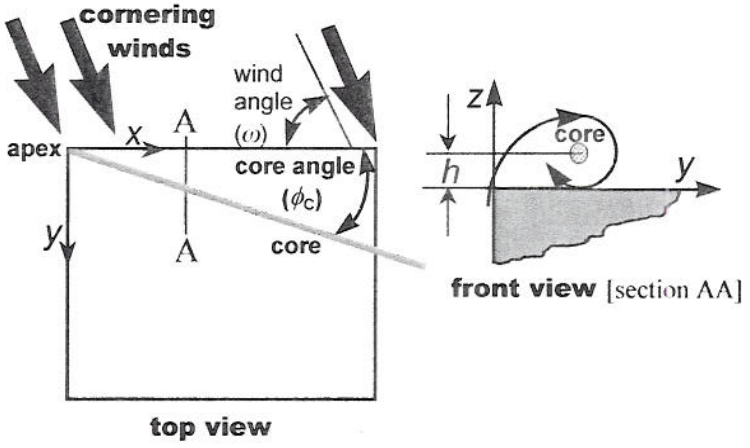

Fig. 3. Vortex position nomenclature.

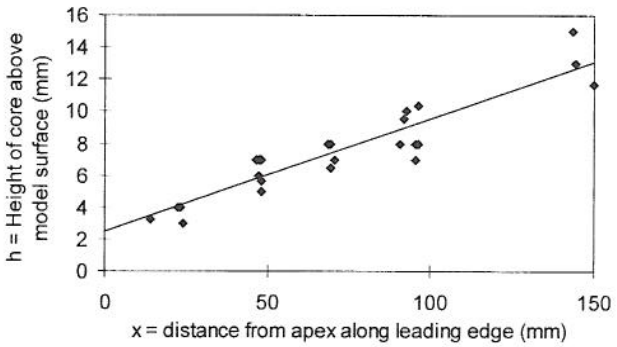

Fig. 4. Finite displacement of vortex core above apex (based upon data from CSU and Refs. [9,11,12]).

leading edge wall are defined as $\omega = 90°$. This differs from some other studies, which define normal winds as 0°.

Vortex position sensitivity tests were carried out for a range of wind speeds. The mean core position was shown to be invariant for speeds from 3 to 10 m/s. For speeds below 3 m/s, $\phi_{\bar{C}}$ increased by 10–20%.

2.2. Digital imaging

The images from the SVHS video recordings proved difficult to quantify, as even in smooth flow, the core would move considerably and the intensity of the smoke would fluctuate. The result was that segments of the visualization would be unusable. By acquiring images digitally and enhancing the contrast as needed, the vortex core position and size could be traced for entire sequences of consecutive images.

The digital recording system makes use of a Pulnix TM-7CN CCD array camera which provides one 640×480 pixel grey-scale image every 1/60th of a second. The camera has a variable shutter speed, providing exposure times ranging from 1/60th of a second to 1/10 000th of a second. The shutter speed was generally set at 1/125th of a second for these tests, so that the image effectively provides an average of the vortex position over this period of time. At a shutter speed of 60 Hz, the cores location was sometimes less discernible as core movement (changes in $\phi_{\bar{C}}$ and h) would blur the image during the exposure time. At speeds above 1/125th, synchronizing the images and the pressure profiles becomes difficult given that both the initial trigger synchronization between the image and pressure sequences, and the variation in the delays between different pressure tap signals, can only be estimated to within 1/500th of a second. (These issues are currently being addressed. See Sections 2.3 and 2.4 below.) Also, at these higher speeds, the intensity of the reflected light was often inadequate, though tests showed that this could be remedied through the use of titanium dioxide smoke and increased laser power to the light sheet.

The camera's 60 Hz video signal was digitized in a Pentium PC using an Imaging Technology Inc. MVC IC Image capture board. Compressed image sequences of up to 6 s could be recorded if the computer's entire 64 MB of RAM were dedicated to image acquisition. Sequences of 4 s were generally used, to leave some memory for

image processing. Real-time image acquisition and processing, as well as batch image file processing, were performed using ITI's Itex-IC c-language libraries. Interactive post processing of the image sequences was performed using the National Institute of Health's free NIH Image program for the Macintosh.

2.3. Pressure measurement

The experiment was moved to the CSU Industrial wind tunnel (IWT), which provides a higher maximum speed than the EWT, thus giving a better signal-to-noise ratio for the pressure measurements. The IWT test section measures 1.8 m × 1.8 m, and test were run at tunnels speeds between 8 and 12 m/s. Initial pressure tests were performed using a 450 mm Plexiglas cube, with a dozen taps located beneath the vortex core under the separated flow (ϕ between 10° and 18°, and values of x ranging from 50 mm to 200 m). These tests confirmed that there is a good correlation of suction fluctuations along this entire surface beneath the vortex [8], indicating that any value of x within the range tested could be used for the pressure/visualization plane. Correlation coefficients between all taps were generally above 0.8, and increased to above 0.95 when the data was low-pass filtered at 10 Hz. Cross-coherence functions remained above 0.5 only for frequencies below 20–30 Hz, confirming that the correlation was due to lower frequency phenomena and indicating that the presence of such phenomena could be observed at the 60 Hz camera frame rate. A sample time series shown in Fig. 5 illustrates one such phenomenon commonly seen in the smooth flow tests: low suction excursions ($|C_p|$ decreases) lasting around 1 or 2 s, and recurring at 2 to 10 s intervals. It will be shown that these excursions can be explained by variations in the vortex size.

A microphone placed in the tunnel revealed that sound peaks at harmonics of 250 Hz were not being adequately damped out by the restrictor tubes. Since the camera is limited to a 60 Hz data rate, and the time series indicated that the presence

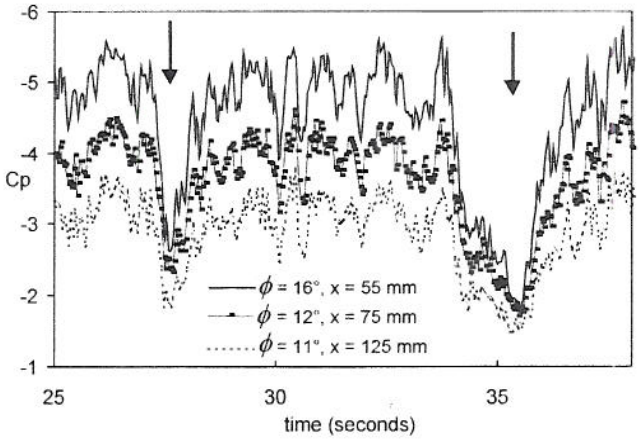

Fig. 5. Pressure time-series excerpt showing two low suction excursions. The data is for a 450 mm surface mounted cube in 10 m/s smooth flow with $\omega = 55$. Tap positions are given in the legend.

of lower frequency phenomena of interest, it was decided to use analog filters to low pass all of the pressure signals at 100 Hz. Three different kinds of filters were used, and each type introduced a signal delay which was measured for a range of sine wave input frequencies. The Krohn Hite filters (models 3323 and 3202) introduced delays of 2 ms at all cutoff frequencies, while the Wavetek model 852's delays increased as the cutoff was reduced. At 100 Hz, the Wavetek's delay was 9 ms. This discrepancy in the delays between taps can pose a problem for the correlation of pressure patterns and vortex image. To counter this, longer restrictor tubes were used for those taps attached to Krohn Hite filters, since the longer tubes also introduce a greater signal delay. All restrictor tubes were designed and tested to provide a linear phase shift out to 200 Hz, and a gain (G_{xy}/G_x) of 1.00 ± 0.01 out to 100 Hz. However, the tube length could not be increased enough to completely compensate for the filter delay discrepancy without undue signal distortion. The net difference in signal delay between any two channels was kept under $\frac{1}{3}$rd of the image sample rate, or 5 ms. These delay differences were both predicted mathematically and measured experimentally to within 2 ms, so they could be partially accounted for during post processing.

It is shown above that the average pressure pattern and low-frequency (< 30 Hz) time series behaviour under the vortex is essentially the same for any value of x near enough to the apex, so that the pressure taps and imaging plane could be located far enough from the apex to allow 1.6 mm ($\frac{1}{16}$th in) taps to be easily drilled near the leading edge. The vertical plane was also selected far enough from the apex to provide a large enough vortex so that its behaviour could be readily observed from outside the tunnel without the help of magnifying lenses, while being close enough to the apex to permit a strong pressure signal to be measured (the pressure drops off exponentially with distance from the apex – see Ref. [1]). A plane normal to the leading edge at $x = 150$ mm was chosen. The row of taps was installed in a cubic aluminium model measuring 450 mm on a side. Eleven taps were drilled at 2.5° intervals, from $\phi = 5°$ to 30°. A 12th tap was installed at $x = 5$ cm and $\phi = 25°$ for comparison. All taps were connected to individual Honeywell Micro Switch transducers mounted inside the model. Pressure data was recorded at 600 Hz.

2.4. Simultaneous pressure measurement and flow visualization

A single external TTL signal was used to trigger both the image sequence acquisition and the pressure time series acquisition. As a result of the camera's internal clock, the start of the image sequence was generally delayed by 8 ms from the start of the pressure time series, though the exact delay could only be estimated to within 2 ms for the best of image sequences. An electronic signature on both the pressure series and the image, as well as a trigger based on the camera's clock cycle, are both being considered for future tests to address this uncertainty.

2.5. Upstream flow conditions

The tests were initially conducted in smooth flow, with no upstream trips, roughness, or spires. The turbulence intensity was measured at 4% at roof height using an LDA probe. These tests have been labelled "smooth flow" in this study.

Some turbulent tests were undertaken, though no atmospheric boundary layer (ABL) simulation was attempted because of the large size of the cubes. Turbulence was generated using individual trips and spires. Model scale experimental results from this study which are labelled "turbulent" (Figs. 7, 8b, 8c, 11a, 12–14, 15a) were taken from runs using a single 200 mm high trip spanning the width of the tunnel, placed 4 m upstream of the model. Rooftop turbulence intensity was 15–20% in this case. A more detailed investigation of the effects of various components and frequencies of incident turbulence is planned for a later stage in the CPWE.

2.6. Full-scale visualization

Three different methods have been successfully employed at TTU for flow visualization in full scale [10]. These methods are the tuft-grid method, the smoke injection technique, and the airfoil-grid method. In all cases, visualizations were more effective at night when floodlights were used for illumination. An 8-mm video camera was used to record the flow in each method. The tuft grid method was employed for the visualization of the corner vortex flow for this paper.

The airfoil-grid makes use of several light-weight airfoils made out of Balsa wood and paper, which are fixed to a metal grid in such a way that they are free to rotate in the plane of the grid. Reflective tape on the sides of the airfoils aids nocturnal visualization. In the tuft grid method, a 20 ft × 7 ft (6 m × 2 m) metal frame with a 6-in (150 mm) grid was used. Coloured yarn segments were tied to the nodes of this grid. For tests close to the apex, a smaller tuff grid (7 ft × 3.5 ft. or 2.1 m × 1.1 m) with a finer mesh size (4 in × 4 in. or 100 mm × 100 mm) was used.

Wind speed and direction data was initially measured at the meteorological tower, located about 50 m from the WERFL building. Later tests made use of a sonic anemometer fixed 1.6 m above the roof apex. This facility is described in detail in Ref. [7].

3. Results

Several authors have presented rooftop pressures, measured along rays from the apex in the vortex region (for example, $\phi = 14^\circ$ in Ref. [1] and $\phi = 16^\circ$ in Ref. [9]) in full ABL simulations. These rays were generally chosen to correspond with the expected location of the ray of maximum suction or the ray of vortex core position. Potential flow theory indicates that these two rays should coincide, since a free point vortex over an infinite plane produces a symmetrical bell-shaped suction curve on the surface of the plane, with the maximum directly beneath the vortex center [8,11,12]. An aerospace literature search performed in Ref. [12] illustrates that this is generally the case for swept delta wings, and the coincidence of ϕ_C and $\phi_{\hat{p}}$ is reported for roof top vortices in Ref. [13], where $\phi_{\hat{p}}$ is defined as in Fig. 6 (taken from Ref. [14]). Similarly, the angles $\phi_{\hat{p}}^{\vee}$ and $\phi_{\sigma_{\hat{p}}}$ can be defined from their respective $C_{\hat{p}}$ contour plots based on the angle ϕ for which $C_{\hat{p}}^{\vee}$ or $C_{\sigma_{\hat{p}}}$ is a maximum for any value of x.

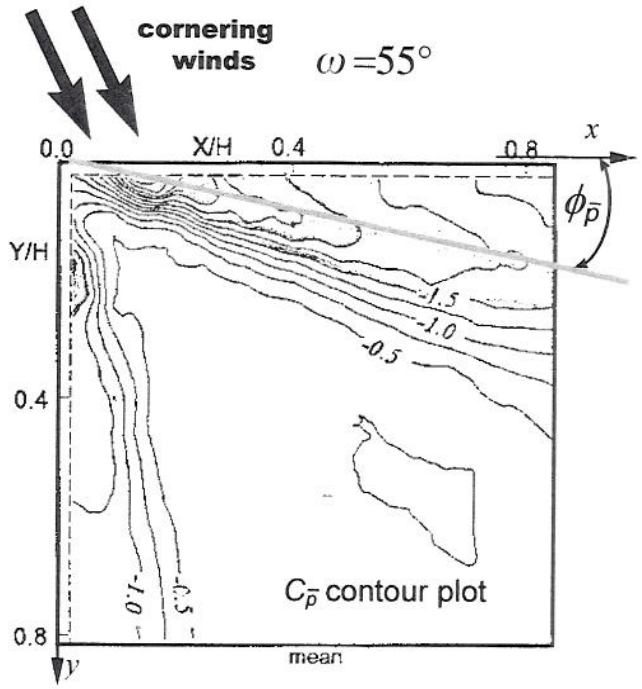

Fig. 6. Angle of maximum mean C_p.

The potential flow theory surface pressure prediction is given by

$$\Delta P = \frac{\Delta P_{\max}}{((r/z_m)^2 + 1)^2}, \tag{1}$$

where z_m is the theoretical vortex height above the surface, r is the distance from the core along the surface and normal to the core axis of rotation, and $\Delta P_{\max}$ is a function of the circulation and z_m. This theory gives the vortex height as

$$z_m = 1.55 y_{1/2}, \tag{2}$$

where $y_{1/2}$ is the half-width of the suction peak. Eq. (2) has been found to hold true for aerospace data, that is for vortices above highly swept wings (included angles less than 40°) at high angles of attack [12].

However, Eq. (2) does not hold true on rooftop vortices, which are more oblong (have a lower h/y_{core} ratio). This is perhaps not too surprising, given the substantial differences between these two flows, notably in the slower axial velocities seen on roofs [11]. Since the circulation is generally unknown (though it has been experimentally measured for delta wings [15]), Eq. (1) becomes merely a curve fitting tool for the surface pressure profile data, where $\Delta P_{\max}$ is either measured or determined from empirical formulae like those in Ref. [1], and z_m is determined from Eq. (2).

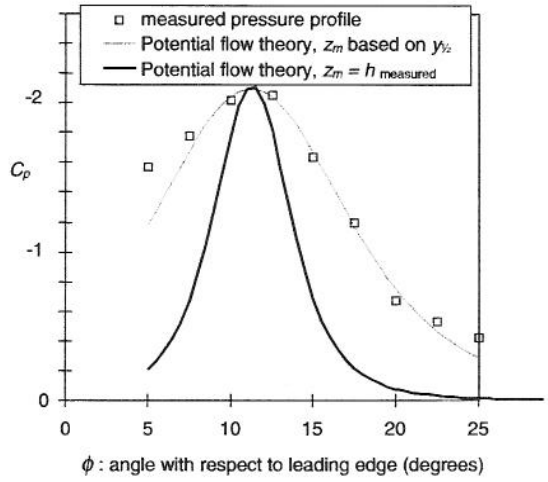

Fig. 7. Pressure profiles, $\omega = 45^\circ$

This curve is fit to a sample average pressure profile in Fig. 7, where ΔP_{max} and r have been corrected to account for the $x = 150$ mm plane not being perpendicular to the vortex core's ray (in this case, $\phi_C = 12^\circ$). Note that the data is asymmetric, with pressures exceeding the curve fit values for $\phi < \phi_C$. This is consistently true for all tests in this study, confirming trends seen in Ref. [8]. Fig. 7 also shows how the potential flow model underpredicts the half-width of the pressure profile if the actual vortex core height is used for z_m.

The profiles for C_{σ_p} and $C_p^{\vee}$ are similarly asymmetric in both turbulent and smooth flow (see Fig. 8). Nonetheless, all of the profiles exhibit clear peaks, which correspond to the values of ϕ_{σ_p}, $\phi_p^{\vee}$, and ϕ_p. Several trends are evident when these angles are compared:

(i) While ϕ_p is slightly lower and $\phi_p^{\vee}$ slightly higher than ϕ_C, these angles of highest suction clearly follow the vortex core position closely.

(ii) ϕ_{σ_p} is greater than ϕ_C for turbulent flow, while being lower for smooth flow.

(iii) Turbulence reduces ϕ_C by around 30%, though the size of this reduction depends on the nature of the turbulence. This agrees with Ref. [8], which gives $\phi_C = 10^\circ$ for turbulent flow and $\phi_C = 13^\circ$ for smooth flow when $\omega = 45^\circ$.

These trends hold true for wind angles from 30° to 70°, as shown in Fig. 9. The ratios between the rays are essentially preserved: ϕ_C/ϕ_p stays nearly constant, while ϕ_{σ_p} remains greater than these two for all values of ω. $\phi_p^{\vee}$ is the exception, remaining in a narrow band between 10° and 16°. This could indicate that for low wind angles, peak suctions are associated with larger than average vortices, while at higher wind angles, peak suctions occur for average or below average-sized vortices.

The curves for ϕ_p, ϕ_{σ_p}, and $\phi_p^{\vee}$ are adapted from Ref. [14], and are all for simulated ABL flow over a 1 : 50 scale model of the WERFL building. The ϕ_C curve is based on

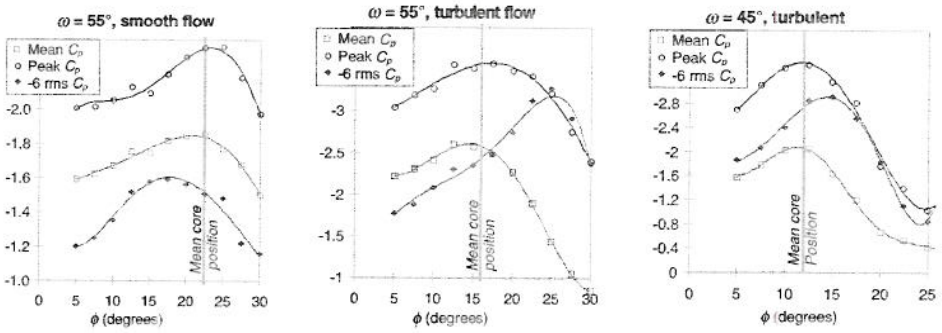

$\phi_p = 21°$	$\phi_p = 15°$	$\phi_p = 11.3°$
$\phi_p^{\vee} = 23.5°$	$\phi_p^{\vee} = 17.5°$	$\phi_p^{\vee} = 11.8°$
$\phi_{\sigma_p} = 18°$	$\phi_{\sigma_p} = 25°$	$\phi_{\sigma_p} = 14.4°$
$\phi_C = 22.5°$	$\phi_C = 16°$	$\phi_C = 12.0°$

Fig. 8. Pressure profiles under various flow conditions, showing relative location of ϕ values.

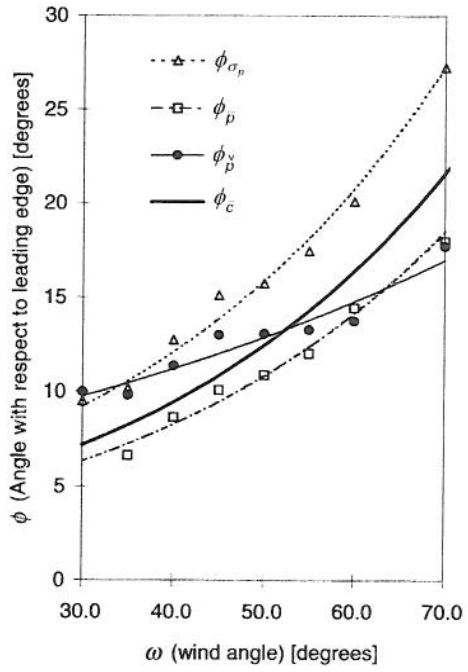

Fig. 9. Relative position of maximum C_p rays and vortex core. Data is from ABL flow. Lines represent exponential curve fits.

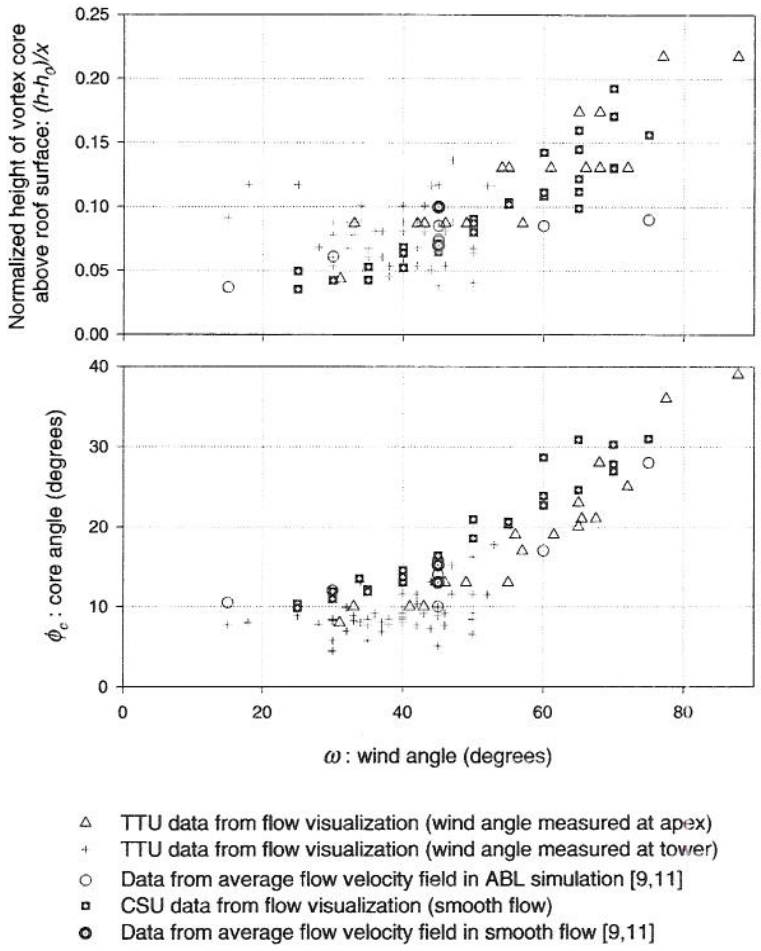

Fig. 10. Vortex core position as a function of wind angle.

the full-scale data presented in Fig. 10b. Fig. 10a shows the vortex core height dependence on ω. The model scale data presented is for smooth flow, illustrating again that ϕ_C decreases in turbulent flow, though h shows little change.

There is also more scatter in the TTU data. This is explained in part by the fact that the TTU data points are single observations, while the model scale data points involve averaged images or averaged flow velocities. The vortex grows and shrinks considerably during a short span of time, as seen in Fig. 11a, which shows all 240 vortex core position observation during a 4 s turbulent flow sequence. The range of motion is decreased for smooth flow (see Fig. 11b), but even so the core is almost equally likely to be found anywhere in the range from $\phi = 20^\circ$ to 26° for $\omega = 55^\circ$.

It is this rapid motion which accounts for ϕ_{σ_p} being larger than ϕ_C in turbulent flow. We see from Fig. 12 that a typical instantaneous pressure profile generally exhibits the same characteristics as the average pressure profile: a gentle loss of suction between

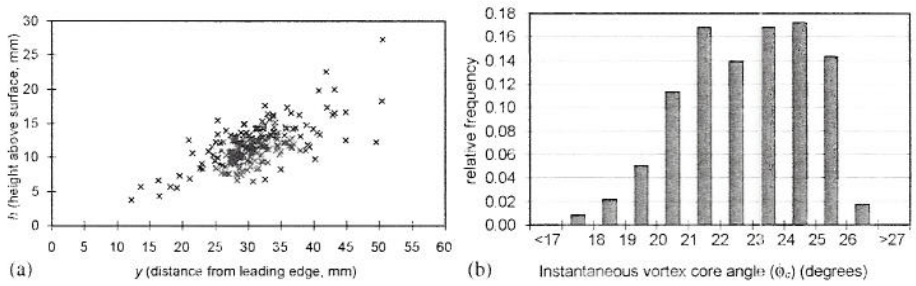

Fig. 11. Vortex core movement during a 4 s long wind tunnel test: (a) turbulent flow, $\omega = 45^{\circ}$; (b) smooth flow, $\omega = 55^{\circ}$.

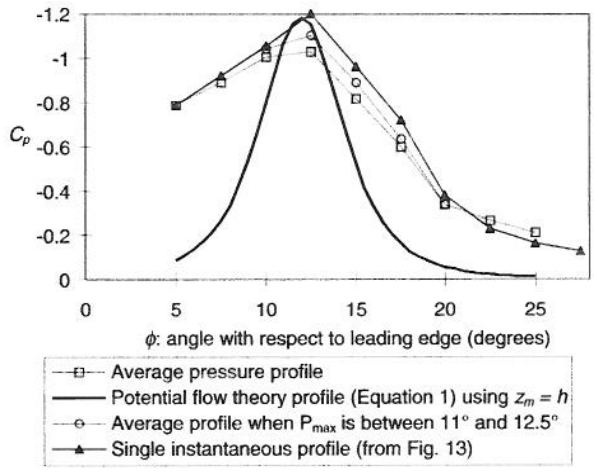

Fig. 12. Surface pressure profiles, $\omega = 45^{\circ}$.

the peak and the wall, with a more rapid loss of suction towards the centre of the roof. Comparison with the image taken simultaneously with this pressure profile shows that this transient pressure peak is located directly beneath the vortex core (Fig. 13). Similar comparisons showed that the peak suction *always* closely follows the moving core. Since the core moves back and forth in ϕ or y, pressure taps beneath the rapid loss of suction inboard of the vortex core ($12.5^{\circ} < \phi < 20^{\circ}$ for turbulent flow and $\omega = 45^{\circ}$) see the greatest fluctuations in suction, as the core approaches and recedes from them, sweeping this high-pressure gradient flow over them. For smooth flow, however, the motion of the vortex is much slower, and ϕ_{σ_p} is not associated with the Cp gradient in the zone between the core and the re-attachment.

This motion might also account for the discrepancy between ϕ_C and ϕ_p. As the vortex moves, regions between the core and the wall ($\phi < \phi_C$) would generally see higher suctions than equidistant regions to the other side of the peak suction, due to the asymmetry of the profile. As a result, the highest mean suction would appear at a point closer to the roof edge than the average vortex position.

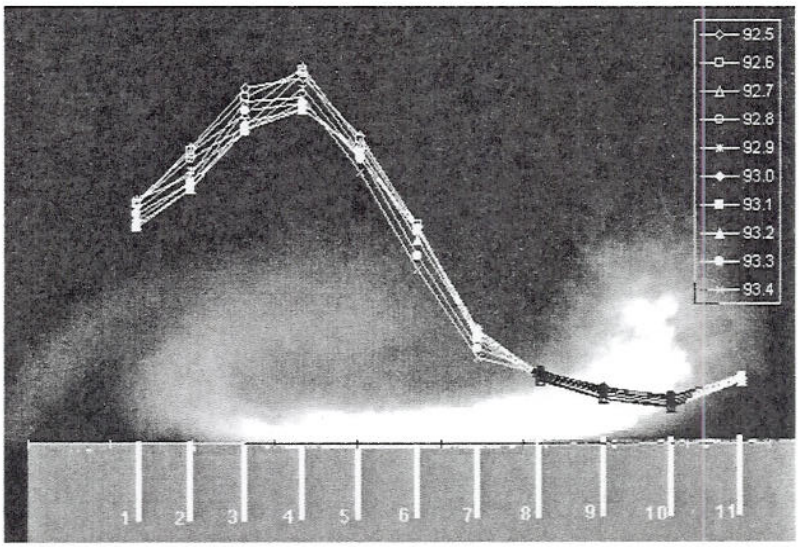

Fig. 13. Vortex image for $\omega = 45°$. The building corner is dark gray, and the pressure taps locations are indicated in white. The 10 surface pressure profiles measured during the image's exposure are superimposed upon the image. $Cp = 0$ at the roof surface. The core is above tap #4 in this picture.

The motion also tends to produce an average pressure profile with smoother peaks and a wider half-width than the individual profiles. However, even the instantaneous profiles with the steepest loss of suction for $\phi > 12.5°$ have a considerably larger half-width than that predicted by potential flow theory, and the average of profiles with Cp_{max} above tap#4 (Fig. 12) shows that the average pressure profile is a reasonably accurate reflection of the typical shape of the instantaneous profiles.

It is important to note that the discussion of typical or averaged characteristics is often too reductive. It has generally proven more instructive to individually examine the image and pressure sequences themselves. It was found that an immediate visual correlation could usually be made between the vortex position and the concurrently recorded surface pressures. To emphasize this connection, the pressure profiles which were measured while an image was being captured have been digitally superimposed on that image. Fig. 13 describes a typical result. Fig. 14 illustrates several flow phenomena, including large suction peaks for both small and large vortices (Fig. 14a and 14b), widely varying profiles for similarly sized vortices (Fig. 14c and 14d), and low suction events where the vortex has essentially disappeared (Fig. 14f). These loss-of-vortex or washout events are only seen for turbulent flow, and are commonly followed by some of the larger suction excursions as the vortex reforms. This "vortex intermittency" is plausibly related to the bi-modal pressure distributions observed for taps beneath the vortices, such as 50501 on the WERFL building [16].

As might be anticipated from the images in Fig. 14, no connection could be established in turbulent flow between suction strength and vortex size except for taps in the range $1.5\phi_C < \phi < 2\phi_C$. These taps are never beneath the core, and experience

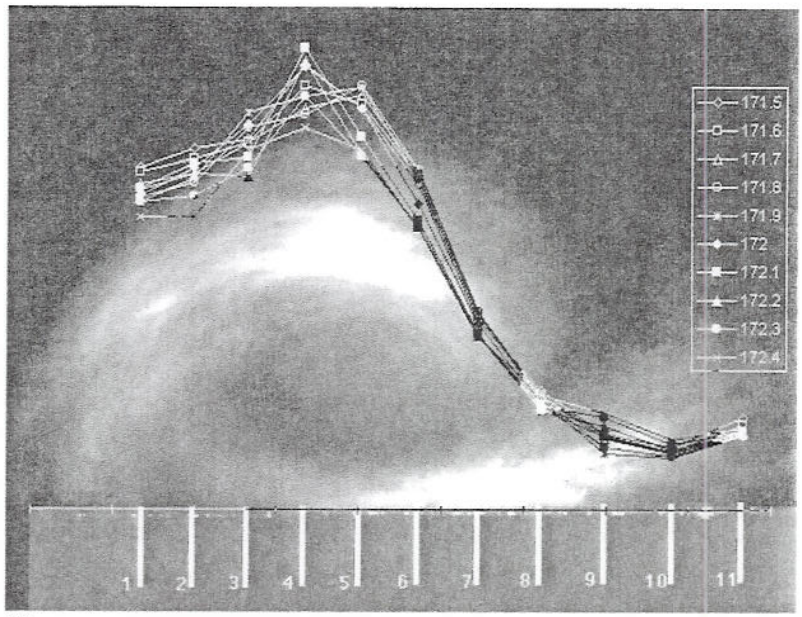

(a)

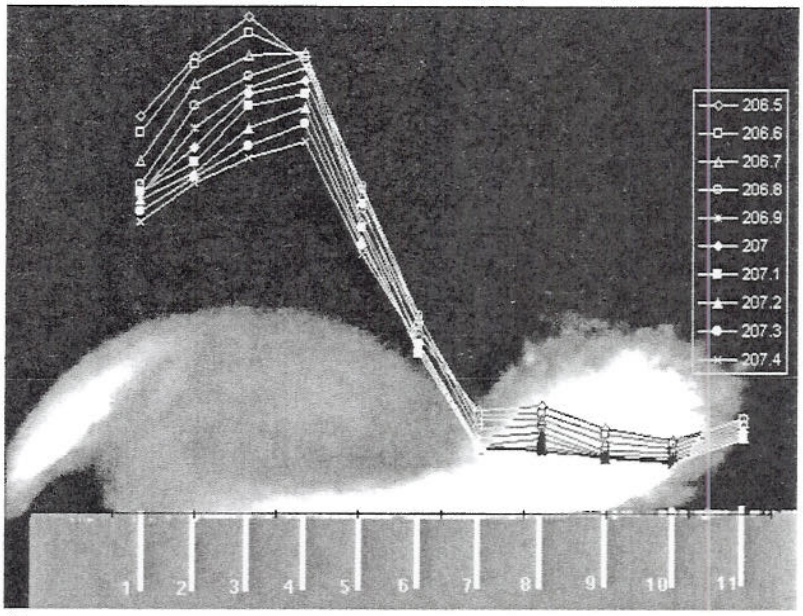

(b)

Fig. 14. Vortex images for $\omega = 45^{\circ}$, with simultaneous pressure profiles.

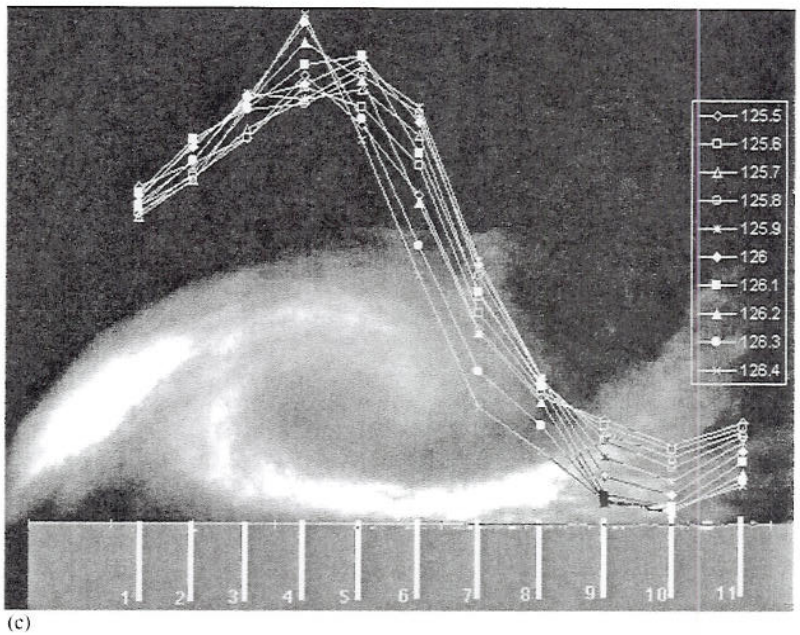

(c)

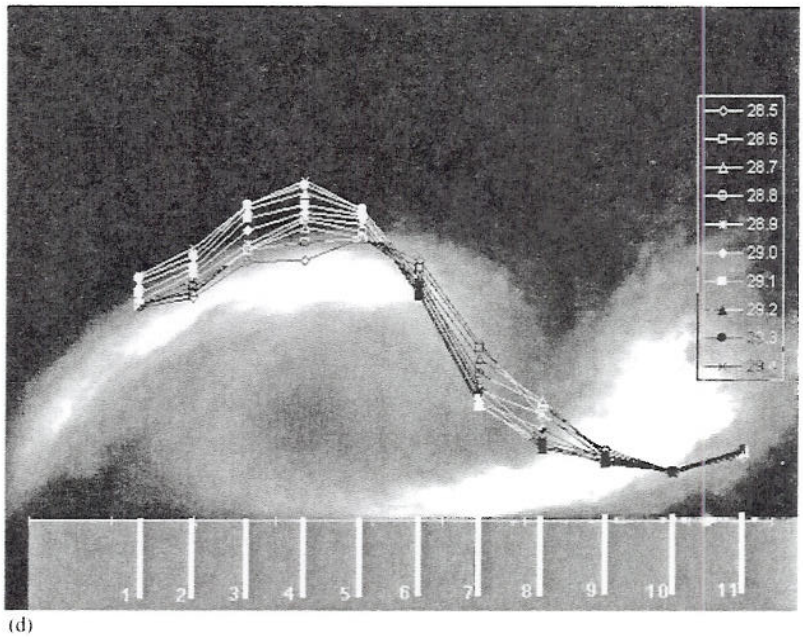

(d)

Fig. 14. Continued.

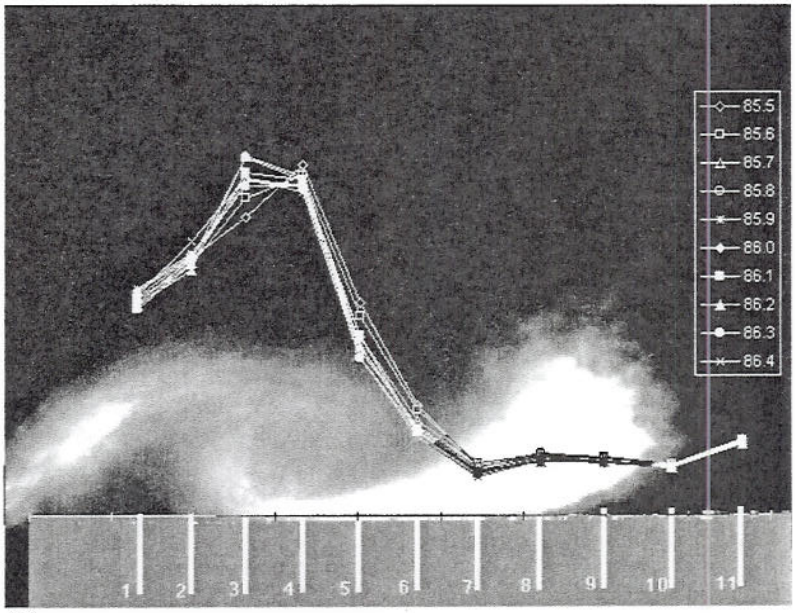

(e)

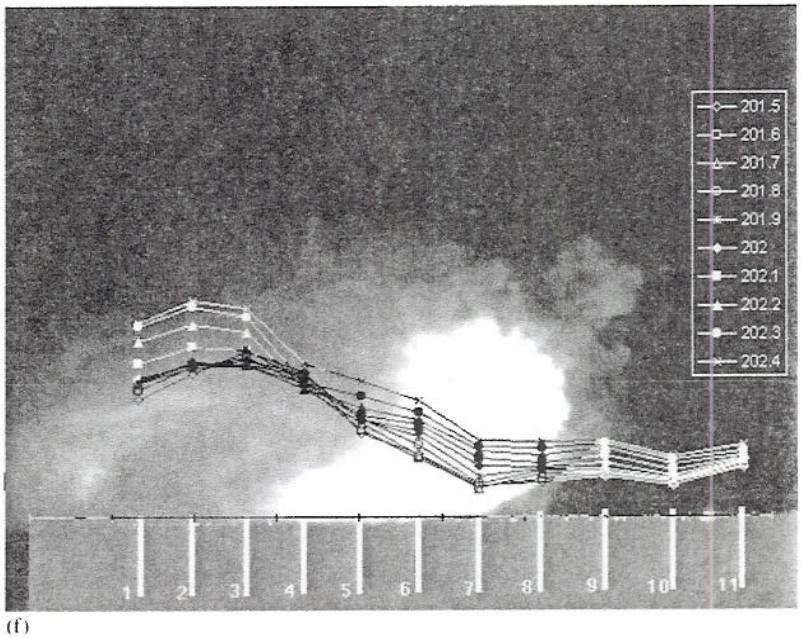

(f)

Fig. 14. Continued.

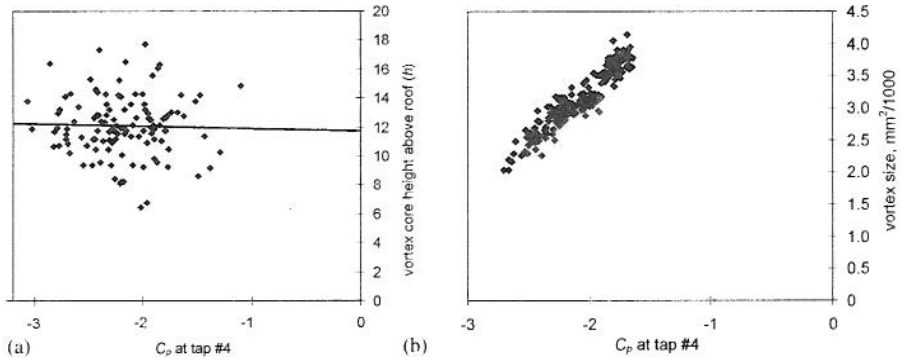

Fig. 15. Dependence of suction on vortex size: (a) turbulent flow, $\omega = 45^\circ$; (b) smooth flow, $\omega = 55^\circ$.

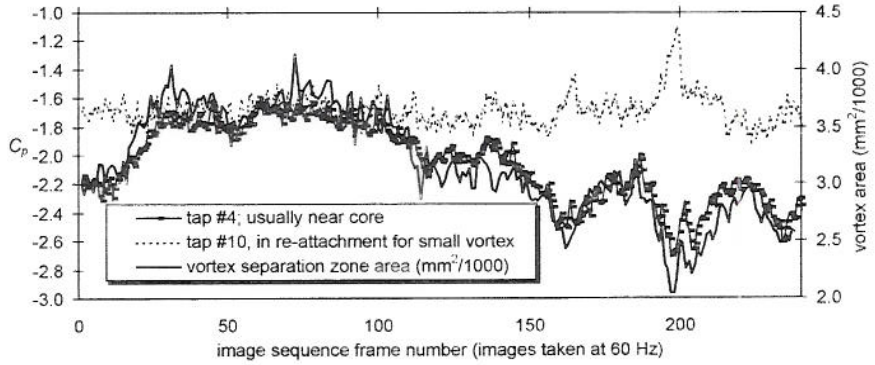

Fig. 16. Pressure coefficient time series (smooth flow, $\omega = 55^\circ$).

greater suctions for larger vortices simply because the core moves towards them as the vortex gets bigger. The actual magnitude of the suction beneath the core was independent of the core's height above the surface, as is evident from Fig. 15a, which shows core height versus suction at a tap located beneath the mean ϕ_c position. Only samples where the core was within $\Delta y = 4$ mm (i.e. $\pm$ 1.5") of this tap are shown. Also shown is the least-squares linear curve fit to this data. The null hypothesis that the slope is zero cannot be rejected with even a 60% level of certainty, and this conclusion does not change for any value of Δy.

Fig. 15b shows that the situation for smooth flow is quite different, as the suction clearly increases linearly as the vortex gets smaller. In this case, vortex size is indicated by the size of the entire separation bubble. By introducing smoke at the apex of the model, the entire separation zone containing the vortex was clouded. The image could then be thresholded so that the separation zone was completely white, and image integration then gives a value for the vortex area.

Fig. 16 is a time series showing how the pressure at a tap near the mean core position follows the vortex size. Correlation coefficients between the vortex size and

the pressures at the highest suction taps were between 0.90 and 0.95. The pressure time series at a tap further from the leading edge is also shown. As with the turbulent flow, such taps have a negative correlation, since suction will decrease far from the leading edge if the core gets small enough (see for example Fig. 16 from frames 150 to 250). The loss of suction incidents seen in Fig. 5, and in Fig. 16 in frames 30–110, are associated with the largest vortices. The flow characteristics governing these aperiodic fluctuations in smooth flow vortex size is currently being investigated.

Why smaller vortices do not produce lower pressures in turbulent flow is not known at this time either. It is hoped that by monitoring the nature of the turbulence and using the non-conventional Cp to remove the effects of local wind speed fluctuations [7], a connection can be established between the orderly vortex-pressure relationship associated with smooth flow, and the more complex interactions seen in turbulent flow.

4. Concluding comments

A facility has been successfully developed to enable the comparison of simultaneously recorded images of a rooftop corner vortex and the pressures beneath this vortex. The initial results confirm that the peak suction lies beneath the vortex core, and moves with the vortex. For smooth flow, the magnitude of this suction peak increases linearly with decreasing vortex size.

The vortex is found to grow larger with increasing wind angle. Increasing turbulence moves the mean vortex core position closer to the leading edge. Considerable motion about the mean position is seen for both smooth and turbulent flow. The combined effects of this motion and the consistent asymmetry of the pressure profile beneath the vortex accounts for the nature of the C_{σ_p} and C_p roof surface pressure patterns.

Acknowledgements

The essential contributions of Dr. Bernd Leitl in developing the laser facilities at CSU are gratefully acknowledged. Dr. D.E. Neff contributed similarly through the development of the pressure data synchronization system. This work is supported by the US National Science Foundation, grant # CMS-9411147 (amendment 007).

References

[1] J.-X. Lin, D. Surry, H.W. Tieleman, The distribution of pressure near roof corners of flat roof buildings, J. Wind Eng. Ind. Aerodyn. 56 (1995) 235–265.

[2] H.W. Tieleman, D. Surry, K.C. Mehta, Full/model scale comparison of surface pressured on the Texas Tech experimental building, J. Wind Eng. Ind. Aerodyn. 61 (1996) 1–23.

[3] H. J. Ham, B. Bienkiewicz, Wind tunnel simulation of TTU flow and building roof pressure, Eighth US National Conference on Wind Engineering, Baltimore,1997.

[4] H.W. Tieleman, D. Surry, J.-X. Lin, Characteristics of mean and fluctuating pressure coefficients under corner (delta wing) vortices, J. Wind Eng. Ind. Aerodyn. 42 (1994) 263–275.
[5] C.W. Letchford, K.C. Mehta, The distribution and correlation of fluctuating pressures on the Texas Tech building, J. Wind Eng. Ind. Aerodyn. 50 (1993) 225–234.
[6] C.W. Letchford, R. Marwood, On the influence of v & w component turbulence on roof pressures beneath conical vortices, Third International Colloquium on Bluff body Aerodynamics and Applications, Blacksburg, VA, 1996.
[7] Z. Zhao, Wind flow characteristics and their effects on low-rise buildings, Ph.D. Dissertation, Civil Engineering, Texas Tech, Lubbock, TX, 1997.
[8] H. Kawai, G. Nishimura, Characteristics of fluctuating suction and conical vortices on a flat roof in oblique flow, J. Wind Eng. Ind. Aerodyn. 60 (1996) 211–225.
[9] R. Marwood, C.J. Wood, Conical vortex movement and its effect on roof pressures, J. Wind Eng. Ind. Aerodyn. 69–71 (1997) 589–595.
[10] P.P. Sarkar, Z. Zhao, K.C. Mehta, Flow visualization and measurement on the roof of the Texas Tech Building, J. Wind Eng Ind. Aerodyn. 69–71 (1997) 597–606.
[11] R. Marwood, An investigation of conical roof edge vortices, D. Phil. Thesis, Lincoln College, University of Oxford, Oxford, UK, 1996.
[12] D.I. Greenwell, N.J. Wood, Determination of vortex location on delta wings from surface pressure measurements, AIAA J. 30 (1992) 2736–2739.
[13] H. Kawai, Structure of conical vortices related with suction fluctuation on a flat roof in oblique smooth and turbulent flows, Third International Colloquium on Bluff Body Aerodynamics and Applications, Blacksburg, VA, 1996.
[14] Y. Sun, Wind loading on loose-laid roofing paver systems, Ph.D. Thesis, Department of Civil Engineering, University of Colorado, Fort Collins, 1993.
[15] K.D. Visser, R.C. Nelson, Measurements of circulation and vorticity in the leading-edge vortex of a delta wing, AIAA J. 31 (1993) 104–111.
[16] L.S. Cochran, Wind tunnel modeling of low-rise structures, Ph.D. Thesis, Civil Engineering, Colorado State University, Fort Collins, CO, 1992, p. 202.